Meccanica (2011) 46: 131–146
DOI 10.1007/s11012-010-9393-x

PARALLEL MANIPULATORS

Kinematic analysis of 5-RPUR (3T2R) parallel mechanisms

Mehdi Tale Masouleh · Clément Gosselin · Mohammad Hossein Saadatzi · Xianwen Kong · Hamid D. Taghirad

Received: 16 September 2009 / Accepted: 29 November 2010 / Published online: 16 December 2010

Abstract This paper investigates some kinematic properties of a five-degree-of-freedom parallel mechanism generating the 3T2R motion and comprising five identical limbs of the RPUR type. The general mechanism originates from the type synthesis performed for symmetrical 5-DOF parallel mechanism. In this study, two classes of simplified designs are proposed whose forward kinematic problem have either a univariate or a closed-form solution. The principal contributions of this study are the solution of the forward kinematic problem for some simplified designs—which may have more solutions than the FKP of the general 6-DOF Stewart platform with 40 solutions—and the determination of the constant-orientation workspace which is based on the topology of the vertex space (Bohemian dome) and a geometric constructive approach.

Keywords 5-DOF parallel mechanisms · Forward kinematic problem · Constant-orientation workspace · Bohemian dome

M. Tale Masouleh (✉) · C. Gosselin
Département de génie mécanique, Université Laval, 1065 Avenue de la Médecine, Québec, QC, Canada, G1V 0A6
e-mail: mehdi.tale-masouleh.1@ulaval.ca

C. Gosselin
e-mail: gosselin@gmc.ulaval.ca

M.H. Saadatzi · H.D. Taghirad
Advanced Robotics & Automated Systems (ARAS), Faculty of Electrical & Computer Engineering, K.N. Toosi University of Technology, P.O. Box 16315-1355, Tehran, Iran

M.H. Saadatzi
e-mail: saadatzi@ee.kntu.ac.ir

H.D. Taghirad
e-mail: Taghirad@kntu.ac.ir

X. Kong
Department of Mechanical Engineering, School of Engineering and Physical Sciences, Heriot-Watt University, Edinburgh, UK, EH14 4AS
e-mail: x.kong@hw.ac.uk

1 Introduction

In general, five-degree-of-freedom (DOF) parallel mechanisms are a class of parallel mechanisms with reduced DOFs which, according to their mobility, fall into three classes: (1) three translational and two rotational freedoms (3T2R), (2) three rotational and two planar translational freedoms ($3R2T_p$) and (3) three rotational and two spherical translational freedoms ($3R2T_s$) [19]. Since, in the industrial context, the 3T2R motion can cover a wide range of applications including, among others, 5-axis machine tools and welding, therefore, in this research, the kinematic properties of this class will be investigated. In medical applications that require at the same time mobility, compactness and accuracy around a functional point, 5-DOF parallel mechanisms can be regarded as a very

promising solution [25]. Recently, the machine tool industry has discovered the potential advantages of parallel mechanisms and many parallel machine tools have been developed based on either the 6-DOF parallel mechanisms (Traditional "Gough-Stewart platform") or asymmetrical 5-DOF parallel mechanisms in which a passive leg constrains the motion of the end-effector [7]. For a comprehensive list of the so-called parallel machine tools in industrial context see [1, 7].

As far as 5-DOF mechanisms with identical limb structures are concerned, researchers have mainly worked on the type synthesis [6, 11, 12, 18, 19, 32]. In fact, it was believed that symmetrical[1] 5-DOF mechanisms could not be built [23] until Huang and Li [10] and Liu et al. in [17] proposed a first architecture. It is worth noticing that most existing 5-DOF parallel manipulators are built using a 5-DOF passive leg which constrains some actuated 6-DOF limbs [5, 21, 31].

To the best knowledge of the authors, up to now, very few kinematic studies have been conducted on symmetrical 5-DOF parallel mechanisms [26, 27, 29, 30]. This is probably due to their short history. The main focuses of this research are the FKP and constant-orientation workspace of symmetric 5-DOF parallel mechanisms, more precisely 5-R$\underline{P}$UR, which can be regarded as one of the most challenging topics in the kinematics of parallel mechanisms[29, 30]. The analytical resolution of the FKP in the context of parallel mechanisms, due to its mathematical complexities, initiated several researches both in mathematics and mechanics. It should be noted that the FKP is solved in polynomial form when it is made equivalent to determining the roots of a univariate polynomial equation [14, 16]. In some cases, upon considering design conditions, such as the coalescence of connection points and planar base and platform, the FKP can be expressed in a closed-form solution, i.e., an explicit solution for the FKP which is a definite asset in practice.

Parallel mechanisms are well-known to have a restricted workspace compared to their counterpart serial manipulators. There is a vast literature on various approaches to obtain the workspace of parallel mechanisms which ranges from discretization algorithms to geometrical approaches [24]. Instead of treating numerically the constant-orientation workspace, the problem is investigated geometrically, i.e., using a *geometric constructive approach* which also provides insight into the optimal design of the mechanism. The central concept of the latter approach is based on the identification of the curves, surfaces and volumes that are obtained by successively releasing the joints from the base to the platform and formulating their connections mathematically. These concepts are either implemented in a computer algebra system or in a CAD system. In this paper, the constant-orientation workspace is investigated by the geometric constructive approach which is inspired from the method proposed in [3, 8] for the computation of the constant-orientation workspace of 6-DOF Gough-Stewart platforms.

Generally, in the workspace analysis, a horizontal or vertical cross section plane is used to reduce the problem to a two-dimensional one. For a large number of parallel mechanisms generating a motion pattern with fewer than 6-DOFs, the latter two cross section planes will not result in homogeneous sections to which algebraic equations can be associated, such as lines, circles ans spheres. Based on the above discussion, the cross section plane proposed for the computation of the constant-orientation workspace of the symmetric 5-DOF parallel mechanisms differs from the classical one mentioned above. The proposed cross section plane in this study, results in a homogeneous section and known geometric objects, such as set of lines and circles and lay down the first step toward applying the algorithm presented in [8].

The remainder of this paper is organized as follows. The architecture and the general kinematic properties of the 5-R$\underline{P}$UR parallel mechanism which originated from the type synthesis performed in [18, 19] are first outlined. The FKP is addressed and from the results obtained two classes of simplified designs—which include in total 9 simplified designs— are found whose FKP have either a univariate or a closed-form solution. The constant–orientation workspace is interpreted geometrically where Bohemian dome comes up and the results are implemented in a CAD system. Moreover, a geometric constructive approach, inspired from the one presented in [8] for the general 6-DOF Stewart platform, is proposed for computing the boundary of the constant-orientation workspace. Based on the latter algorithm, the volume of the constant–orientation workspace is obtained and plotted with respect to the two permitted rotational DOFs.

[1] In the context of this paper, the symmetric properties refer to the limb type and not to the geometry, such as centro–symmetrical simplifications.

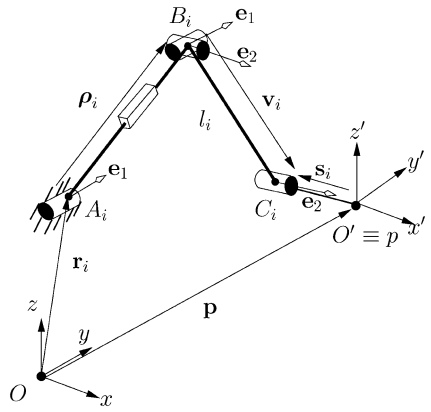

Fig. 1 Schematic representation of a RPUR limb

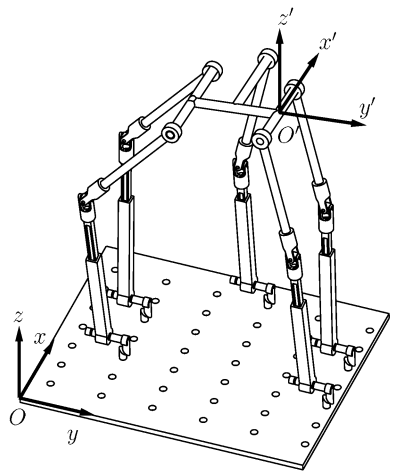

Fig. 2 CAD model of a 5-RPUR parallel mechanism

2 Architecture, kinematic modeling

2.1 Architecture

Figures 1 and 2 provide respectively a representation of a RPUR limb and a CAD model for a 5-DOF parallel mechanism providing all three translational DOFs, plus two independent rotational DOFs (3T2R) of the end-effector, namely (x, y, z, ϕ, θ). In the latter notation, (x, y, z) are the components of vector $\mathbf{p}$ and represent the translational DOFs with respect of the fixed frame O, illustrated in Fig. 1, and (ϕ, θ) stand for the orientation DOFs around axes x and $y(\mathbf{e}_1)$, respectively. The rotation from the fixed frame O_{xyz} to the moving frame $O'_{x'y'z'}$ is defined as follows: a first rotation of angle ϕ is performed around x-axis followed by the second rotation about $\mathbf{e}_1$ by angle θ.

The input of the mechanism is provided by the five linear prismatic actuators. From the type synthesis presented in [18], the geometric characteristics associated with the components of each limb are as follows: The five revolute joints attached to the platform (the last R joint in each of the limbs) have parallel axes, the five revolute joints attached to the base have parallel axes, the first two revolute joints of each limb have parallel axes and the last two revolute joints of each limb have parallel axes. It should be noted that the second and third revolute joints in each limb are built with intersecting and perpendicular axes and are thus assimilated to a U (Universal) joint. In addition, the direction of the P joint is perpendicular to the axes of its adjacent R joints. As mentioned above, the 5-RPUR is a limited-DOF parallel mechanism which cannot rotate about any axis that is parallel to $\mathbf{e}_2 \times \mathbf{e}_1$, where $\mathbf{e}_1$ and $\mathbf{e}_2$ are unit vectors respectively along the axes of the first (and second) and third (and fourth) revolute joints of the ith limb, as illustrated in Fig. 1.

2.2 Kinematic modeling

Referring to Fig. 1, a fixed reference frame $O - xyz$ is attached to the base of the mechanism with $\mathbf{i}$, $\mathbf{j}$ and $\mathbf{k}$ as its unit vectors and a moving reference *frame* or *mobile frame*, $O - x'y'z'$, is attached to the moving platform. In this paper the superscript $'$ stands for a vector representation in the mobile frame. In the ith limb, the extension of the actuated prismatic joint is measured with respect to a reference point A_i, located on the axis of the first revolute joint, by the joint coordinate ρ_i which is the signed distance between point A_i and a reference point B_i on the U joint ($A_iB_i \perp \mathbf{e}_1$). Vector $\mathbf{e}_{\rho i}$ is in turn defined as a unit vector in the direction of the prismatic joint and therefore the vector connecting point A_i to point B_i can be written as $\boldsymbol{\rho}_i = \rho_i \mathbf{e}_{\rho i}$. Point B_i is defined as the intersection of the axes of the second and third revolute joints of the ith limb. Vector $\mathbf{r}_i$ (a constant vector) is defined as the position vector of point A_i in the fixed reference frame. Similarly, vector $\mathbf{s}_i$ is the vector connecting point O' of the platform to a reference point C_i on the axis of the last revolute joint of the ith limb. Vector $\mathbf{v}_i$ is the vector connecting point B_i to point C_i ($B_iC_i \perp \mathbf{e}_2$). Since in the proposed architecture vectors $\mathbf{e}_1$ and $\mathbf{e}_2$ are orthogonal $\mathbf{e}_1 \cdot \mathbf{e}_2 = 0$. Finally, the position of the platform is represented by vector $\mathbf{p} = [x, y, z]^T$ connecting point O to point O' and the orientation of the moving frame with respect to the fixed frame is given by a rotation matrix $\mathbf{Q}$.

It should be noted that $\mathbf{Q}$ cannot be prescribed arbitrarily since the mechanism has only two degrees of rotational freedom. Therefore, a rotation matrix consistent with the orientation capabilities of the mechanism must be chosen. To this end and for simplicity, the reference frames attached respectively to the base and to the platform are chosen such that $\mathbf{e}'_2 = [1, 0, 0]^T$ and $\mathbf{e}_1 = [0, 1, 0]^T$, Fig. 2. Hence, based on the results presented in [27] and on the definition of angles ϕ and θ given above, this rotation matrix can be written as:

$$\mathbf{Q} = \begin{bmatrix} \cos\theta & \sin\phi\sin\theta & \cos\phi\sin\theta \\ 0 & \cos\phi & -\sin\phi \\ -\sin\theta & \sin\phi\cos\theta & \cos\phi\cos\theta \end{bmatrix}. \tag{1}$$

For a given value of the angles ϕ and θ, matrix $\mathbf{Q}$ is readily computed and vectors $\mathbf{s}_i$ and $\mathbf{e}_2$ are then obtained as:

$$\mathbf{s}_i = \mathbf{Q}\mathbf{s}'_i, \qquad \mathbf{e}_2 = \mathbf{Q}\mathbf{e}'_2 = [\cos\theta, 0, -\sin\theta]^T. \tag{2}$$

3 Forward kinematic problem (FKP)

The FKP pertains to finding the pose of the platform for a given set of actuated joints. With reference to Fig. 1, the following equations, arising from the kinematic constraint of the ith limb, can be written:

$$(x_{Bi} - x_{Ai})^2 + (z_{Bi} - z_{Ai})^2 = \rho_i^2, \tag{3}$$

$$(x_{Ci} - x_{Bi})^2 + (y_{Ci} - y_{Bi})^2 + (z_{Ci} - z_{Bi})^2 = l_i^2, \tag{4}$$

$$(x_{Ci} - x_{Bi})\cos\theta - (z_{Ci} - z_{Bi})\sin\theta = 0, \tag{5}$$

such that the first two equations represent, respectively, the magnitude of $\boldsymbol{\rho}_i$ and $\mathbf{v}_i$ and the last one corresponds to the kinematic constraints between $\mathbf{e}_2$ and $\mathbf{v}_i$, i.e., $\mathbf{e}_2 \perp \mathbf{v}_i$.

For the FKP, the above system of equations should be solved for (x, y, z, ϕ, θ) with respect to input data which are the lengths of the prismatic actuators, ρ_i.

The set of (3)–(5) contains intermediate variables, or passive variables, which are the coordinates of the two passive joints, namely B_i and C_i. Since C_i is attached to the platform, its coordinates can be written directly in terms of the platform pose. One has:

$$[x_{Ci}, y_{Ci}, z_{Ci}]^T = \mathbf{p} + \mathbf{Q}\mathbf{s}'_i. \tag{6}$$

As the complete solution to the system of the equations for the FKP, (3)–(5), $i = 1, \ldots, 5$, is quite challenging, [28, 29] numerous approaches were proposed in the literature and practice including the use of numerical procedures, simplifying the mechanism by the coalescence of some of the connection-points on the platform or the base and, finally, to use some extra sensors. Similarly, in this project, simplifying the mechanism by the coalescence of some of the connection-points is considered for solving the FKP with the aim of obtaining a simpler design, reducing the mechanical interferences and increasing the workspace volume.

From the results obtained in [27], the following conclusion can be drawn: *Any mechanical simplification which provides the coordinates of two pairs of U joints explicitly or a relation among them leads to a univariate solution for the FKP.* The above issue remains central to the development of the simplified designs having either a univariate or a closed-form solution to the FKP. With the above conclusion in mind, consider two limbs, i and j, for which:

1. The connection points at the base, A_i and A_j, are in a plane with $\mathbf{e}_1$ as normal or coincide;
2. Both second moving links have the same length, $l_i = l_j$, or coincide;
3. The connection points on the platform, C_i and C_j, are aligned with $\mathbf{e}_2$, or coincide.

From the solution to the IKP presented in [27], it follows that the above conditions result in a simplified arrangement for which both second moving links are parallel, $\mathbf{v}_i \parallel \mathbf{v}_j$, and the line connecting B_i to B_j is aligned with $\mathbf{e}_2$. Consequently, in such a design there is a relation between two of the U joints, i.e., the line connecting them is aligned with $\mathbf{e}_2$ which implies that:

$$x_{Bj} - x_{Bi} = (s_j - s_i)\cos\theta, \tag{7}$$

$$z_{Bj} - z_{Bi} = (s_i - s_j)\sin\theta, \tag{8}$$

where s_i is a geometric parameter of the platform representing the x component of $\mathbf{s}'_i$, the vector connecting the limb to the mobile frame, i.e., C_i to O'. Therefore, in a design for which two pairs of limbs fulfil the latter conditions, on the basis of the above conclusion, the FKP admits a univariate solution. There are three distinct situations, $\mathcal{S} = \{\mathcal{A}_1\mathcal{A}_2\mathcal{A}_3\}$, in which the latter conditions described above can occur as depicted in Fig. 3. Therefore, all second order subsets of $\mathcal{S}$ adopt a polynomial form for their FKP, namely:

$$\begin{aligned} &\{\{\mathcal{A}_1\mathcal{A}_1\}, \{\mathcal{A}_1\mathcal{A}_2\}, \{\mathcal{A}_1\mathcal{A}_3\}, \\ &\{\mathcal{A}_2\mathcal{A}_3\}, \{\mathcal{A}_2\mathcal{A}_2\}, \{\mathcal{A}_3\mathcal{A}_3\}\}. \end{aligned} \tag{9}$$

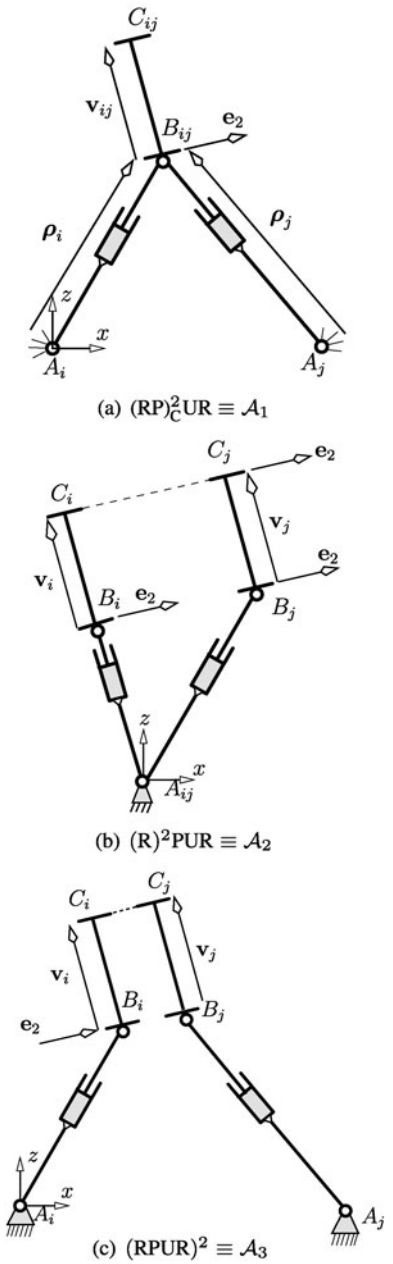

Fig. 3 Simplified kinematic arrangements

For instance, a $\{\mathcal{A}_1\mathcal{A}_2\}$ design is a 5-DOF parallel mechanism which consists of two simplified arrangements of type $\mathcal{A}_1$ and $\mathcal{A}_2$ plus a regular RPUR limb free of design constraints. Figure 4 presents a CAD model of a $\{\mathcal{A}_1\mathcal{A}_1\}$ design. As it can be observed, the U joints in B_{12} and B_{34} are designed in such a way that there is an offset between the axes, which leads to a reduction in the mechanical interferences and hence a

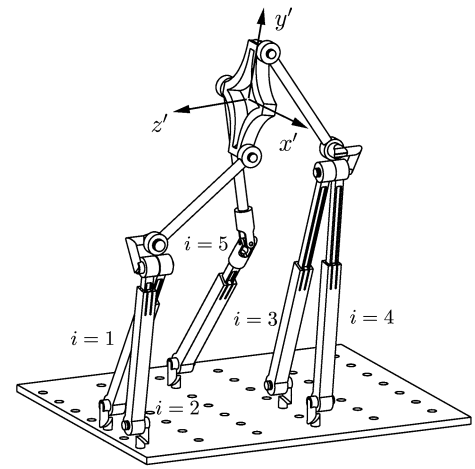

Fig. 4 CAD model of a $\{\mathcal{A}_1\mathcal{A}_1\}$ parallel mechanism

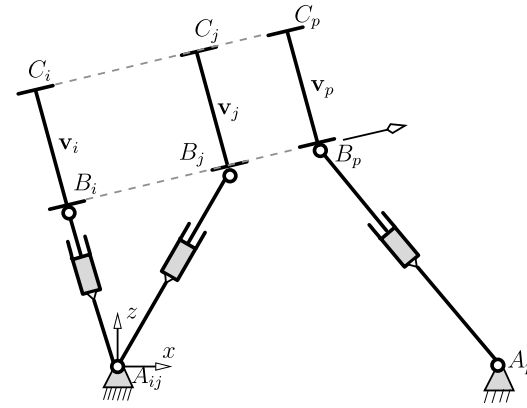

Fig. 5 A $\{\mathcal{M}_p\mathcal{A}_2\}$ arrangement

large travel for the joints. In such a situation, although the joint is no longer a U joint per se, the kinematic model given above remains valid. From (9) it follows that a $\{\mathcal{A}_3\mathcal{A}_3\}$ design, Fig. 2, is free of any coalescence of connection points and comparing with other designs presented above could be regarded as the most general design having a univariate solution for the FKP.

There is a second class of 5-RPUR parallel mechanisms whose FKP has a closed-form solution and can be formulated as follows:

$$\{\{\mathcal{M}_p\mathcal{A}_1\}, \{\mathcal{M}_p\mathcal{A}_2\}, \{\mathcal{M}_p\mathcal{A}_3\}\} \tag{10}$$

where $\mathcal{M}_p$ is a limb which, together with its accompanying simplified arrangement satisfies the latter conditions. Figure 5 depicts schematically a $\{\mathcal{M}_p\mathcal{A}_2\}$ design and it can be observed that $\mathbf{v}_i \parallel \mathbf{v}_j \parallel \mathbf{v}_p$. Although

the two remaining limbs could be placed arbitrarily, they should not belong to $\mathcal{S}$, i.e., $\{\mathcal{M}_p\mathcal{A}_i\mathcal{A}_j\}$, because it would result in an *architecturally singular mechanism*. In the following section, the FKP of three simplified designs, $\{\mathcal{A}_1\mathcal{A}_1\}$, $\{\mathcal{A}_1\mathcal{A}_2\}$ and $\{\mathcal{M}_p\mathcal{A}_2\}$, which belong to (9) and (10) are investigated.

3.1 Closed-form solution for the FKP of a $\{\mathcal{A}_1\mathcal{A}_1\}$ design

Figure 4 represents a CAD model for a $\{\mathcal{A}_1\mathcal{A}_1\}$ design. Referring to Fig. 4(a), the coordinates of the U joints belonging to the simplified arrangement $\mathcal{A}_1$, B_{12} and B_{34}, can be readily computed and consist of the intersection of two circles centered at A_1 and A_2 (A_3 and A_4) with radius ρ_1 and ρ_2 (ρ_3 and ρ_4). Four solutions can be found as a whole for the coordinates of the latter U joints. Having in place the coordinates of these two joints and upon subtracting (5) for $i = 1, 2$ from $i = 3, 4$ leads to:

$$(x_{B34} - x_{B12})\cos\theta - (z_{B34} - z_{B12})\sin\theta = (s_{34} - s_{12}). \tag{11}$$

Then applying the approach proposed in [20] for solving an equation having the general form of $a\cos\theta + b\sin\theta = c$, results in the following for θ:

$$\theta = \arccos\left(\frac{s_{12} - s_{34}}{\sqrt{(x_{B34} - x_{B12})^2 + (z_{B34} - z_{B12})^2}}\right) + \operatorname{atan2}(z_{B12} - z_{B34}, x_{B34} - x_{B12}). \tag{12}$$

From the above it can be deduced that θ have up to $2 \times 4 = 8$ solutions (2 and 4 stand respectively for the number of solution for θ and for the number of solution for the coordinates of the two U joints, B_{12} and B_{34}).

Moreover, by inspection of (11), it is clear that when $x_{B34} - x_{B12} = z_{B34} - z_{B12} = (s_{34} - s_{12}) = 0$ then the FKP admits infinitely many solutions for θ and the mechanism exhibits a singularity which can be classified as a *self-motion* [15]. In such a configuration the first axes, $\mathbf{e}_1$, of both U joints belonging to the simplified arrangement are aligned. Based on the *Grassmann line geometry*, this singularity is a *hyperbolic congruence*. The details concerning the determination of singular configurations of this kind of manipulators by means of the so-called *Grassmann line geometry* is presented in [26].

Having determined the value of θ and the coordinates of both U joints, the next step consists in computing the coordinates of the U joint belonging to the regular limb, B_5. Skipping mathematical derivations, (3) for $i = 5$ can be re-written with respect to the obtained values and solved for x_{B5} as follows:

$$x_{B5} = x_{A5}\sin^2\theta + \mathcal{L}_5\cos\theta \pm \sin\theta\sqrt{\rho_5^2 - (x_{A5}\cos\theta - \mathcal{L}_5)^2}, \tag{13}$$

where

$$\mathcal{L}_5 = x_{B1}\cos\theta - z_{B1}\sin\theta + (s_5 - s_1). \tag{14}$$

From the above it can be concluded that two sets of solutions can be found for (x_{B5}, z_{B5}). Reaching this step, all the passive variables, B_i, and one unknown for the FKP, θ, are known. From Fig. 4, it can be seen that in a $\{\mathcal{A}_1\mathcal{A}_1\}$ design the loop $B_{12}C_{12}C_{34}B_{34}$ can be made equivalent to a 4-bar linkage. This result is valid for all $\{\mathcal{A}_i\mathcal{A}_j\}$ designs. As it is well-known, the motion of a 4-bar linkage generates a *sextic*, i.e., a sixth order curve [13]. Thus, in such a design, the FKP corresponds to the intersection of the sextic and a circle centred at B_5 which is generated by the regular limbs. From Bezout's theorem, it follows that this intersection results in $2 \times 6 = 12$ intersection points including two circular imaginary points as triple points [22]. Thus the intersection of the sextic and the circle results in up to $2 \times 6 - 2 \times 3 = 6$ real intersection points (2 stands for the degree of the circle, 6 for the sextic and 3 for the imaginary points) which are the solutions for the set (x, y, z, ϕ). From the above it is known that two solution is possible for the position of B_5. Taking account all the above factors, for one given value of θ the FKP of this mechanism results in $6 \times 2 = 12$ solutions. Since the 4-bar linkages can be constructed upon 8 ways then the upper bound for the number of postures of the FKP is $12 \times 8 = 96$. This results is consistent with the expression obtained by direct manipulation of the equations which is omitted here.

3.2 Closed-form solution for the FKP of a $\{\mathcal{A}_1\mathcal{A}_2\}$ design

Figures 6 and 7 respectively show the schematic representation of the base and moving platform and the CAD model of a $\{\mathcal{A}_1\mathcal{A}_2\}$ design. As it can be observed from Fig. 6, two moving frames $O'(x, y, z)$

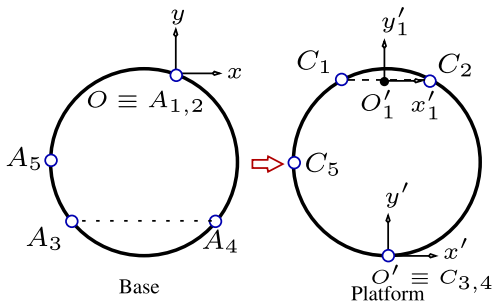

Fig. 6 Schematic representation of the base and platform for a $\{\mathcal{A}_1\mathcal{A}_2\}$ parallel mechanism

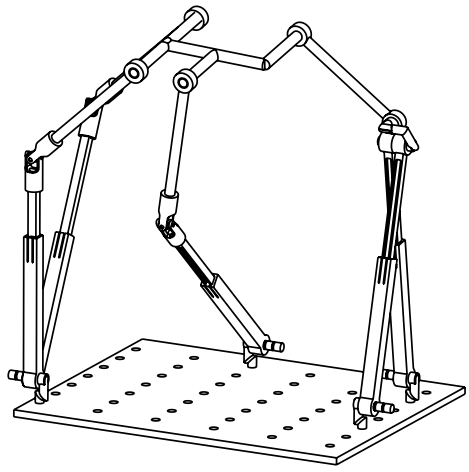

Fig. 7 CAD model of a $\{\mathcal{A}_1\mathcal{A}_3\}$ parallel mechanism

and $O_1'(x_1, y_1, z_1)$, are considered in such a way that the line connecting them is perpendicular to $\mathbf{e}_2$, i.e., $O'O_1' \cdot \mathbf{e}_2 = 0$:

$$(x - x_1)\cos\theta - (z - z_1)\sin\theta = 0. \tag{15}$$

Re-writing (4) and (5) for the limbs belonging to $\mathcal{A}_2$, $i = 1, 2$, one has:

$$(x_1 - x_{B1})^2 + (y_1 - y_{B1})^2 + (z_1 - z_{B1})^2 = s_1^2 + l_1^2, \tag{16}$$

$$(x_1 - x_{B2})^2 + (y_1 - y_{B2})^2 + (z_1 - z_{B2})^2 = s_2^2 + l_1^2. \tag{17}$$

Subtracting (16) from (17) leads to:

$$2x_1(x_{B2} - x_{B1}) + 2z_1(z_{B2} - z_{B1}) = s_1^2 - s_2^2 + x_{B2}^2 + z_{B2}^2 - (x_{B1}^2 + z_{B2}^2). \tag{18}$$

It should be noted that due to the $\mathcal{A}_2$ arrangement, we have $y_{B1} = y_{B2}$ which leads to the y component vanishing as a whole in the rest of analysis. Subtracting (3) for $i = 2$ from the one with $i = 1$ results in:

$$x_{B2}^2 + z_{B2}^2 - (x_{B1}^2 + z_{B2}^2) = \rho_2^2 - \rho_1^2. \tag{19}$$

For this design, (7) and (8) hold for $i = 1, 2$, and one has:

$$x_{B2} - x_{B1} = (s_2 - s_1)\cos\theta, \tag{20}$$

$$z_{B2} - z_{B1} = -(s_2 - s_1)\sin\theta. \tag{21}$$

Substituting (19)–(21) into (18) leads to:

$$x_1\cos\theta - z_1\sin\theta = \frac{\rho_2^2 - \rho_1^2 + s_1^2 - s_2^2}{2(s_2 - s_1)}. \tag{22}$$

For the $\mathcal{A}_1$ arrangement, $i = 3, 4$, one could write (5) as follows:

$$x\cos\theta - z\sin\theta = x_{B34}\cos\theta - z_{B34}\sin\theta. \tag{23}$$

It should be noted that $B_{34}(x_{B34}, y_{B34}, z_{B34})$ is a known point for the FKP. Having in mind that (15) holds, subtracting (22) from (23) leads to:

$$x_{B34}\cos\theta - z_{B34}\sin\theta = \frac{\rho_2^2 - \rho_1^2 + s_1^2 - s_2^2}{2(s_2 - s_1)}. \tag{24}$$

Then applying the approach proposed in [20] for solving an equation having the general form of $a\cos\theta + b\sin\theta = c$ results in the following for θ:

$$\theta = \arccos\left(\frac{\rho_2^2 - \rho_1^2 + s_1^2 - s_2^2}{2(s_2 - s_1)\sqrt{x_{B34}^2 + z_{B34}^2}}\right) - \operatorname{atan2}(z_{B34}, x_{B34}). \tag{25}$$

Moreover, for a configuration for which $x_{B34} = z_{B34} = 0$, which implies that both prismatic actuators corresponding to $\mathcal{A}_1$ are aligned, then the FKP admits infinitely many solutions for θ and consequently the mechanism exhibits a singularity which can be regarded as a *self-motion*.

Since two solutions can be found for the coordinates of B_{34}, in general four solutions are possible for θ. It can be shown that for a given θ and B_{34} one solution can be found for B_1 and B_2 corresponding to the $\mathcal{A}_2$ arrangement. Reaching this step, similarly to what was done for the previous mechanism, the FKP can be solved for the remaining variables (x, y, z, ϕ).

As mentioned previously, $\{\mathcal{A}_1\mathcal{A}_2\}$ can be regarded as a 4-bar linkage. Thus, upon considering the circle generated by the last limb, 6 solutions can be found for a given θ. In summary, since up to 4 solutions are in hand for θ, upon considering the two solutions for B_5, the FKP has up to 48 solutions.

3.3 Closed-form solution for the FKP of a $\{\mathcal{M}_p\mathcal{A}_2\}$ design

The FKP of this simplified design is explored based on the known solution of the FKP of the 3-RPR planar parallel mechanism [9] and results obtained in the previous section for the FKP of a $\{\mathcal{A}_1\mathcal{A}_1\}$ design. From Fig. 5, the lower loop constituted by $A_{ij}B_iB_jB_pA_pA_{ij}$ can be made equivalent to a 3-RPR planar parallel mechanism. It is well-known that a general planar 3-RPR parallel mechanism has up to 6 real solutions for the FKP. However, considering some design conditions may reduce this upper bound. Such design conditions are presented in [9] where it is revealed that the equivalent 3-RPR parallel mechanism, due to the linear base and platform, have up to four solutions. This implies that four solutions can be found for θ. As mentioned previously, there exists two limbs which are free of any design conditions. By considering one of these two limbs together with the three limbs constituting the $\{\mathcal{M}_p\mathcal{A}_2\}$ design, one may imagine again a 4-bar linkages. Hence, the sextic coming from the FKP of the 4-bar linkage intersects the circle generated by the last limb in 6 points. Thus the upper bound for the number solutions becomes: $6 \times 2 \times 2 \times 4 = 96$ solutions (6 for the 4-bar linkage, 2 for B_4, 2 for B_5 and 4 for θ).

4 Workspace determination

The complete workspace of the 5-RPUR manipulator can be regarded as a five-dimensional space for which no visualization exists. In the context of parallel mechanism workspace, one representation that is often used is *the constant-orientation workspace*, which is the set of locations of the moving platform that can be reached with a given prescribed orientation [24]. Geometrically, the problem of determining the constant-orientation workspace for a limb of the 5-RPUR parallel mechanism can be regarded as follows: For a fixed elongation of the prismatic actuator, the first revolute joint provides a circular trajectory centred at A_i with ρ_i as radius. The second link generates a surface by sweeping a second circle, with $\mathbf{e}_2$ as axis, along the first circle. Since the direction of $\mathbf{e}_2$ is prescribed and must remain constant, such a surface is a quadratic surface and is called a *Bohemian dome* [3]. This quadratic surface can be generated by moving a circle that remains parallel to a plane along a curve that is perpendicular to the same plane, as shown in Fig. 8. Once this surface is obtained, it should be extruded along the axis of the prismatic actuator, which converts the surface to a volume. The above geometrical interpretation for the limb workspace of a RPUR is fully explained in [27] but a CAD model for a constant-orientation workspace is not presented. Upon following the procedures described above and in [27, 30], a CAD model for the constant orientation of a RPUR limb can be found and is referred to here as $\mathcal{B}_i$. The challenge is with the extension of the Bohemian dome to the vertex space where the stroke of the actuator is taken into account [27, 30]. Moreover, one of the most common issues for all the vertex spaces of symmetric 5-DOF parallel mechanisms is the fact that the topology of the vertex space is influenced by the value of θ. The vertex space of a RPUR parallel mechanism have up to three holes:

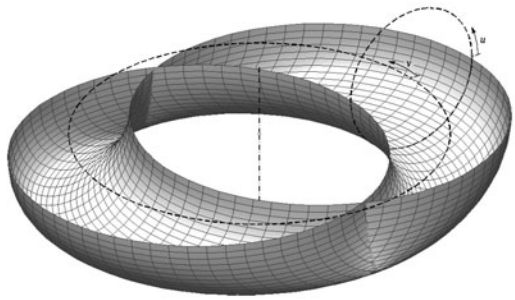

Fig. 8 The lower half of a Bohemian dome, taken from [3]

1. $\mathcal{H}_1$: Always exists and it can be obtained by considering the upper and lower parts of the Bohemian dome generated by $\rho_{\max}$, Fig. 9;
2. $\mathcal{H}_2$: Sweeping $\mathcal{S}_3$ around the fixed circle, by having the Bohemian dome concept, $\rho_{\min}$ with A_i as centre and then cut all the objects located after the plane $\mathcal{Q}_1$, Fig. 10;
3. $\mathcal{H}_3$: Exists when $\frac{\Delta\rho_i}{2} < l_i$ and comes from the intersection of the upper parts of the Bohemian domes generated by $\rho_{\max i}$ and $\rho_{\min i}$, Fig. 11.

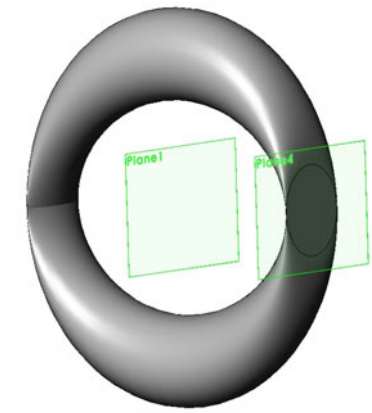

(a) The upper and lower parts of the Bohemian dome generated by $\rho_{\max i}$

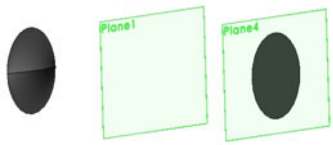

(b) Their intersections

Fig. 9 The $\mathcal{H}_1$ hole

These are the holes which should be removed from the main body presented in Fig. 12 in order to obtain the vertex space, Fig. 13, called $\mathcal{B}_i$. For the main body, in Fig. 12, one should sweep $\mathcal{S}_4$ around the fixed circle centred at A_i with $\rho_{\max}$ as radius. Then only objects located in upper side of $\mathcal{Q}_2$ are kept.

Following the same method as in [8] the workspace of a limb attached to a platform can be computed by applying an offset vector to the limb workspace, $\mathcal{B}_i$, where this vector is opposed to the vector connecting the mobile platform to the limb. In the present case, this offset vector is $-\mathbf{s}_i$. Finally, the workspace of the mechanism is found by intersecting five $\mathcal{B}_i$ which are offset by their corresponding $-\mathbf{s}_i$. Figure 14, obtained with a CAD system, Solid works , represents an example for the constant-orientation workspace of a 5-RPUR parallel mechanism, which consists of the intersection of five offset $\mathcal{B}_i$, whose design parameters are presented in Table 1. In this section, for all mechanisms, it is assumed that $l_i = 150$ mm, $\rho_{\min} = 250$ mm and $\rho_{\max} = 400$ mm. It should be noted that the mechanical interferences are omitted in this study.

Similarly, Fig. 15 represents the constant orientation workspace of a $\{\mathcal{A}_1\mathcal{A}_1\}$ design, with design parameters presented in Table 2.

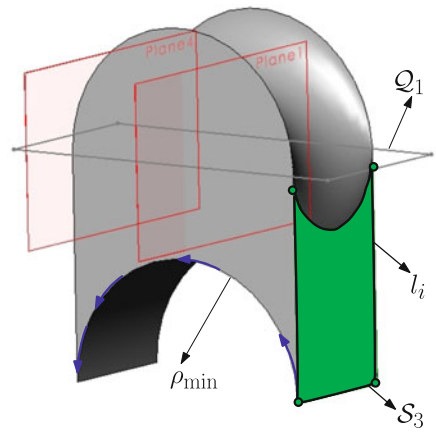

(a) Sketch to obtain $\mathcal{H}_2$

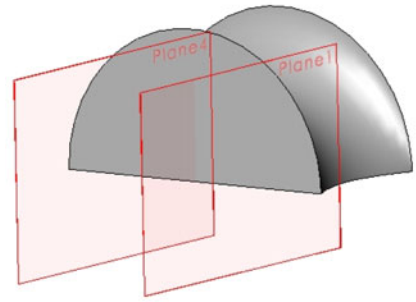

(b) Final result

Fig. 10 The $\mathcal{H}_2$ hole

Handling the topology of the constant-orientation workspace of each limb, the so-called *vertex space*, $\mathcal{B}_i$, makes it easy to model in a CAD system but there are some drawbacks to this approach [2]. One of the most important drawbacks is due to the fact that the working modes cannot be introduced in a CAD system. In what follows, an approach, inspired from the algorithm proposed in [8], is proposed which brings insight into the problem and is very useful during the design stage [4].

Being aware that each vertex space $\mathcal{B}_i$ should be offset by $-\mathbf{s}_i$, then, mathematically, this offset can be expressed as follows:

$$\mathbf{w}_i = \mathbf{r}_i - \mathbf{Q}\mathbf{s}_i'. \tag{26}$$

Since in the case of the constant-orientation workspace we are dealing with a three-dimensional space, a cross sectional plane should be considered in order to reduce the problem to a two dimensional one. From a geometrical inspection, it follows that a cross sectional plane, called $\mathcal{X}_i$, which is rotated around the y-axis of the

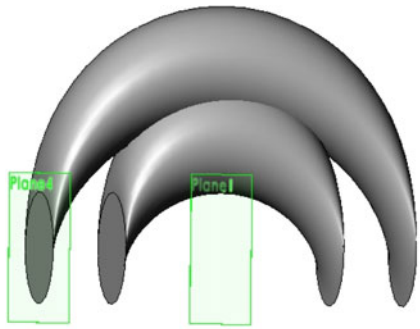

(a) The upper parts of the Bohemian domes generated by $\rho_{\max i}$ and $\rho_{\min i}$

(b) Their intersection

Fig. 11 The $\mathcal{H}_3$ hole

fixed frame by angle θ results in a homogeneous section for the $\mathcal{B}_i$ and to conventional geometric objects such as circles and lines. This helps to reduce the complexity of the computation and, to be precise, leads to an algorithm which consists in finding the intersection of some known geometric objects such as intersections of circles and lines. It can be shown that the equation of each line leads to $\mathcal{K}_i = (\mathbf{s}_i + \mathbf{p} - \mathbf{r}_i) \cdot \mathbf{e}_1 \geq 0$ which is the inequality constraint of the IKP [27].

This particular cross section implies that (26) should be multiplied by $\mathbf{Q}_{y,\theta}^{-1}$ where $\mathbf{Q}_{y,\theta}$ is the rotation around the y axis by angle θ:

$$\mathbf{w}_i' = \mathbf{Q}_{y,\theta}^{-1}\mathbf{w}_i = \mathbf{Q}_{y,\theta}^{-1}\mathbf{r}_i - \mathbf{Q}_{x,\phi}\mathbf{s}_i', \tag{27}$$

where $\mathbf{Q}_{x,\phi}$ is the rotation matrix around the x-axis by angle ϕ. The next step consists in obtaining the interval for which the cross sectional plan should be applied in order to avoid non-essential cross sections. This can be done by considering Fig. 16 which represents schematically a $\mathcal{B}_i$ for a $x' - z'$ view. From Fig. 16, it can be seen that two different Bohemian domes are constituting the $\mathcal{B}_i$: (1) $\mathcal{B}_{\max i}$ coming from $\rho_{\max i}$ and (2) $\mathcal{B}_{\min i}$ coming from $\rho_{\min i}$. In what follows, we tempt to find algebraic conditions which describes the boundary conditions for $\mathcal{H}_2$. For $\mathcal{H}_1$ and $\mathcal{H}_3$, due to space limitation, we refer to study presented in [30] which is based on a numeric verification of IKP.

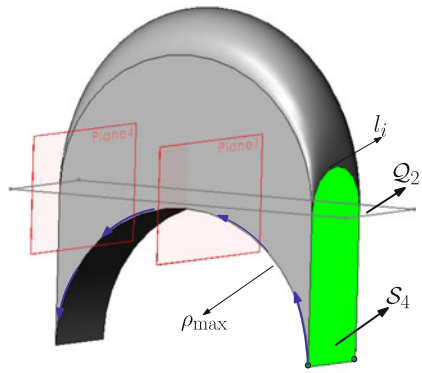

(a) Sketch to obtain the main body

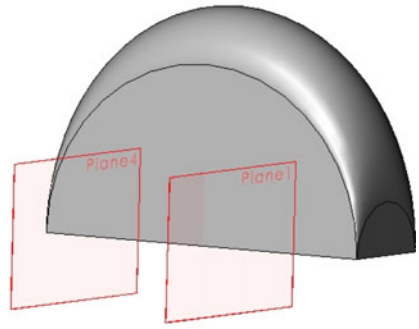

(b) Intersecting with the grey plane

Fig. 12 The main body

From 16 it follows that $\mathcal{X}_i$ crosses all the $\mathcal{B}_{\max i}$ iff it lies inside of this interval:

$$\max(w_{ix}' - \rho_{\max i}) \leq x_H' \leq \min(w_{ix}' + \rho_{\max i}),$$
$$i = 1, 2, \ldots, 5 \tag{28}$$

where $\mathbf{w}_i' = [w_{ix}', w_{iy}', w_{iz}']^T$. Similarly, it can be confirmed that each, and not all, $\mathcal{B}_{\min i}$ crosses $\mathcal{X}_i$ iff:

$$w_{ix} - \rho_{\min i} \leq x_H' \leq w_{ix} + \rho_{\min i}. \tag{29}$$

From (28) and (29), it can be concluded that for a given $\mathcal{X}_i$ passing through x_H' it is possible that certain circles of $\mathcal{B}_{\min i}$ are crossed while all the circles of $\mathcal{B}_{\max i}$ are crossed. As mentioned previously, the defined cross sectional plane, $\mathcal{X}_i$, results in a homogeneous section for which the obtained circles in each section have the same radius. However, the centre of the circles changes for different $\mathcal{X}_i$. These centres should be obtained separately for the circles obtained by crossing $\mathcal{B}_{\min i}$ and $\mathcal{B}_{\max i}$ by $\mathcal{X}_i$. Skipping mathematical derivations, these centres can be obtained as follow:

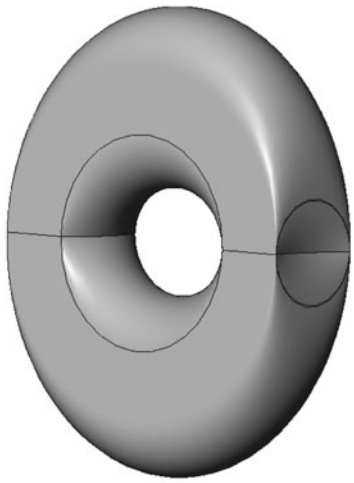

(a) The whole

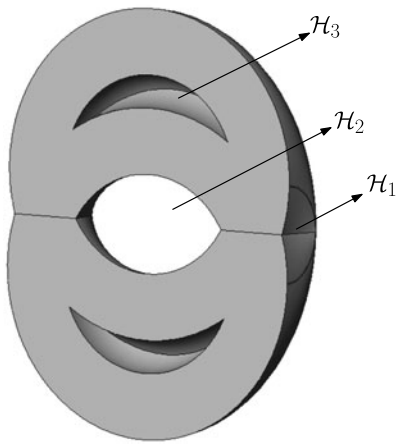

(b) The cross-section

Fig. 13 The most general vertex space of a RPUR limb, $\mathcal{B}_i$, having the three holes

1. For $\mathcal{B}_{\min i}$:
   - The lower circle:

$$\mathbf{c}'_l = \big[x'_H, w'_{iy}, w'_{iz} - \sqrt{\rho^2_{\min i} - (w'_{ix} - x'_H)^2}\,\big]^T. \tag{30}$$

   - The upper circle:

$$\mathbf{c}'_u = \big[x'_H, w'_{iy}, w'_{iz} + \sqrt{\rho^2_{\min i} - (w'_{ix} - x'_H)^2}\,\big]^T. \tag{31}$$

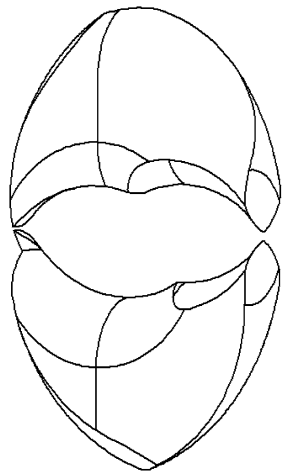

Fig. 14 Constant-orientation workspace for the design presented in Table 1 for $\phi = 0$ and $\theta = 0$

Table 1 Geometric properties (in mm) assumed for a general 5-RPUR

i	$(\mathbf{r}_i)_x$	$(\mathbf{r}_i)_y$	$(\mathbf{r}_i)_z$	$(\mathbf{s}'_i)_x$	$(\mathbf{s}'_i)_y$	$(\mathbf{s}'_i)_z$
1	−55	30	50	−50	0	0
2	245	30	50	50	0	0
3	20	205	0	0	50	0
4	200	180	0	0	50	−50
5	0	0	0	0	−50	−50

2. For $\mathcal{B}_{\max i}$:
   - The lower circle:

$$\mathbf{C}'_l = \big[x'_H, w'_{iy}, w'_{iz} - \sqrt{\rho^2_{\max i} - (w'_{ix} - x'_H)^2}\,\big]^T. \tag{32}$$

   - The upper circle:

$$\mathbf{C}'_u = \big[x'_H, w'_{iy}, w'_{iz} + \sqrt{\rho^2_{\max i} - (w'_{ix} - x'_H)^2}\,\big]^T. \tag{33}$$

Reaching this step, the problem of obtaining the constant-orientation workspace of a 5-RPUR parallel mechanism is made equivalent to the determination of the constant-orientation of the 6-DOF Gough-Stewart platform, i.e., finding the intersections of twelve circles, for a given horizontal cross section, and whether they belong to the constant orientation workspace [8].

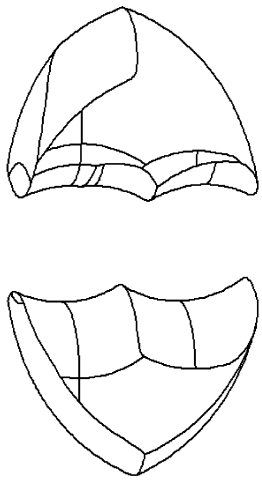

Fig. 15 Constant-orientation workspace for the design presented in Table 2 for $\phi = 0$ and $\theta = 0$

Table 2 Geometric properties (in mm) assumed for a $\{\mathcal{A}_1\mathcal{A}_1\}$ design

i	$(\mathbf{r}_i)_x$	$(\mathbf{r}_i)_y$	$(\mathbf{r}_i)_z$	$(\mathbf{s}'_i)_x$	$(\mathbf{s}'_i)_y$	$(\mathbf{s}'_i)_z$
1	0	0	0	0	−50	0
2	245	0	0	0	−50	0
3	−50.8	127	−50.8	0	50	0
4	203.2	127	−50.8	0	50	0
5	−101.6	50.8	0	−50	0	0

The algorithm presented in [8] for the 6-DOF parallel mechanisms is not fully developed here and only some issues are presented which should be inevitably considered in order to find the constant-orientation workspace of a 5-RPUR parallel mechanism.

Having determined the centre of all circles and the position of the lines, their intersections should be found which consist of the intersections of:

1. circles due to $\mathcal{B}_{\min i}$
2. circles due to $\mathcal{B}_{\max i}$
3. circles due to $\mathcal{B}_{\min i}$ and $\mathcal{B}_{\max i}$
4. circles due to $\mathcal{B}_{\min i}$ and the lines $\mathcal{K}_i = 0$
5. circles due to $\mathcal{B}_{\max i}$ and the lines $\mathcal{K}_i = 0$

Figure 17 shows a cross section at $x'_H = 50$ mm for a design whose geometrical parameters are presented in Table 1, for $\phi = \frac{\pi}{4}$ and $\theta = \frac{\pi}{4}$. From the number of possible point intersections, it can be deduced that the arrangement of these intersections in order to identify which ones constitute the boundary of the workspace should be a delicate task. The last step consists in obtaining all the circular arcs and lines defined by the intersection points found above by ordering these points. This should be accompanied by a checking procedure to identify the arcs and lines that constitute the boundary of the workspace. To do so, for a given curve(line or circle portion), belonging to a given $\mathcal{B}_i$, a point lying on the curve is chosen, preferably not one of the end points. Then, it is verified that whether or not this point is located inside all the other $\mathcal{B}_{\max i}$ and outside all the other $\mathcal{B}_{\min i}$. This can be regarded as the most challenging part of the workspace determination that should be elaborated with care and is fully explained in [8]. The CAD model presented above provides some insight into the particular situations for these verification. Consider $\mathcal{T} = (x_t, y_t, z_t)$ to be a mid-point lying on a given arc found in the previous step which could be a candidate for the boundary of the workspace. Skipping mathematical derivations, one has:

$$a_1 = z_t - \big(C'_{lz} - \sqrt{l_i^2 - (y_t - C'_{ly})^2}\big), \tag{34}$$

$$a_2 = z_t - \big(C'_{uz} + \sqrt{l_i^2 - (y_t - C'_{uy})^2}\big), \tag{35}$$

and the criterion for which $\mathcal{T}$, and consequently its corresponding arc, is inside of the all the $\mathcal{B}_{\max i}$ is:

$$\{a_1, a_2\} \in \mathbb{R}, \quad a_1 > 0,\ a_2 < 0. \tag{36}$$

Referring to (32) and (33), $C'_l(C'_{lx}, C'_{ly}, C'_{lz})$ and $C'_u(C'_{ux}, C'_{uy}, C'_{uz})$ stand respectively for the centres of the circles obtained from $\mathcal{B}_{\max i}$. Similarly, the same can be obtained for being outside of a $\mathcal{B}_{\min i}$ and it follows that:

$$a_1 = z_t - \big(c'_{lz} + \sqrt{l_i^2 - (y_t - c'_{ly})^2}\big), \tag{37}$$

$$a_2 = z_t - \big(c'_{uz} - \sqrt{l_i^2 - (y_t - c'_{uy})^2}\big), \tag{38}$$

and the criterion for which $\mathcal{T}$, and consequently the corresponding arc, is outside of a $\mathcal{B}_{\min i}$ is that one of the following conditions is *not* satisfied:

$$\{a_1, a_2\} \in \mathbb{R}, \quad a_1 > 0,\ a_2 < 0. \tag{39}$$

In the above, $c'_l(c'_{lx}, c'_{ly}, c'_{lz})$ and $c'_u(c'_{ux}, c'_{uy}, c'_{uz})$ stand for respectively the centre of the circles presented in (30) and (31). It is noted that when two circles originating from $\mathcal{B}_{\min i}$ are intersecting then

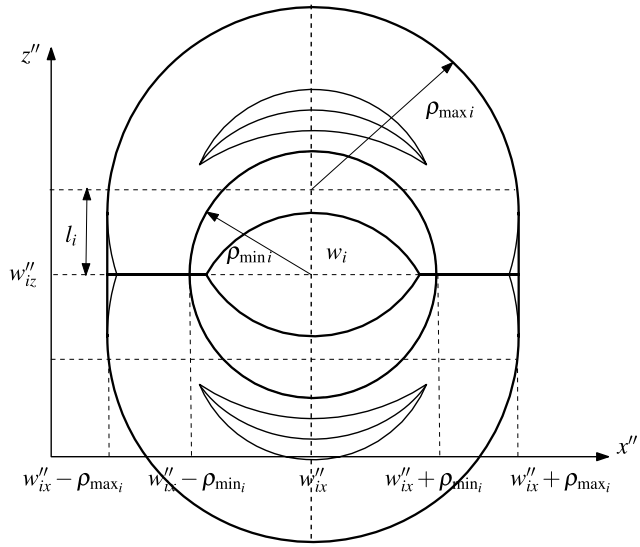

Fig. 16 A schematic representation of a $\mathcal{B}_i$ including the used parameters

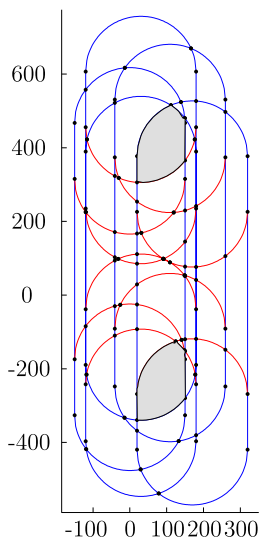

Fig. 17 Cross section at $x'_H = 50$ mm of five $\mathcal{B}_i$ and the possible intersections among them

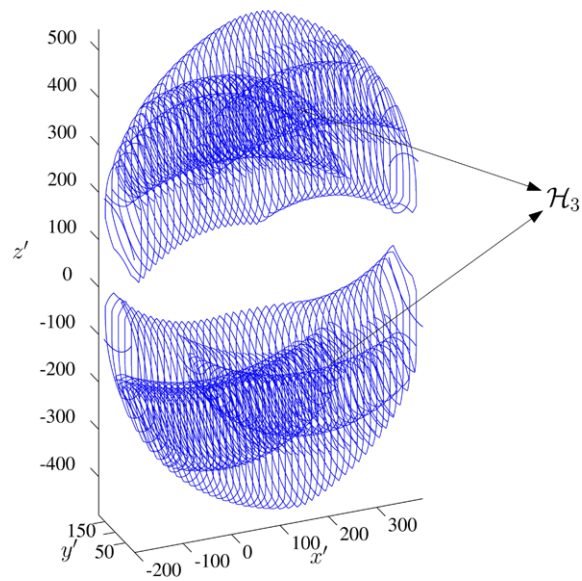

Fig. 18 Constant-orientation workspace for the design presented in Table 1 for $\phi = \theta = 0$

the curve connecting the two intersection points is excluded and should not be considered as a boundary of the constant-orientation workspace.

Finally, applying the above procedure for different x'_H leads to obtaining the constant-orientation workspace in three-dimensional space. Figure 18 represents the constant-orientation workspace for a design presented in Table 1 for $\phi = \theta = 0$ and it can be seen that it is the same that is found with the CAD system in Fig. 14. Figure 19 shows also the constant-orientation workspace for the design presented in Table 2 which corresponds to a $\{\mathcal{A}_1\mathcal{A}_2\}$ design. In Figs. 18 and 19 all the three holes are present and $\mathcal{H}_1$ and $\mathcal{H}_3$ are obtained using the approach presented in [30]. It should be noted that for the sake of clarity holes due to $\mathcal{H}_3$ are omitted respectively for Figs. 14 and 15.

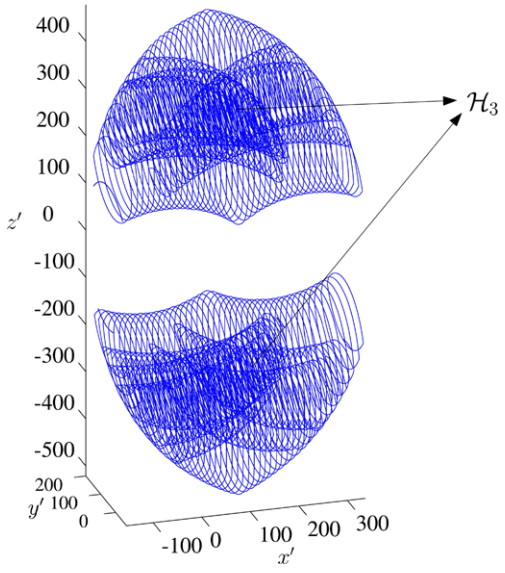

Fig. 19 Constant-orientation workspace for the design presented in Table 2, $\{\mathcal{A}_1, \mathcal{A}_2\}$ for $\phi = \theta = 0$

As elaborated in [8], reaching this step the volume of the constant-orientation workspace can be obtained. The technique is essentially based on the *Gauss Divergence Theorem* which can be applied to planar regions. As mentioned previously, the constant-orientation workspace for a given cross section consists of the intersection of circles, resulting in some arcs, and lines. Thus, in order to compute the area, $\mathcal{D}_i$, for a given section the area created by both arcs and lines should be considered. Based on results obtained in [8], apart from some minor modifications, the area created by an arc—with centre of curvature as $[h, g]^T$, its radius of curvature r and the angle corresponding to the end points θ_1 and θ_2, (not to be confused with θ for DOF)—can be written as:

$$\mathcal{D}_i = hr[\sin\theta_2 - \sin\theta_1] + gr[\cos\theta_1 - \cos\theta_2] + r^2[\theta_2 - \theta_1]. \tag{40}$$

In what concerns the area created by the lines $\mathcal{K}_i = 0$, based on the formulation given in [8] for the *Gauss Divergence Theorem*, it can be expressed as follows:

$$\mathbf{n} = \begin{cases} [0, -1]^T & \text{for the left side boundary,} \\ [0, 1]^T & \text{for the right side boundary,} \end{cases} \tag{41}$$

$$\mathbf{s} = \begin{cases} [y'_l, z']^T & \text{for the left side boundary,} \\ [y'_r, z']^T & \text{for the right side boundary.} \end{cases} \tag{42}$$

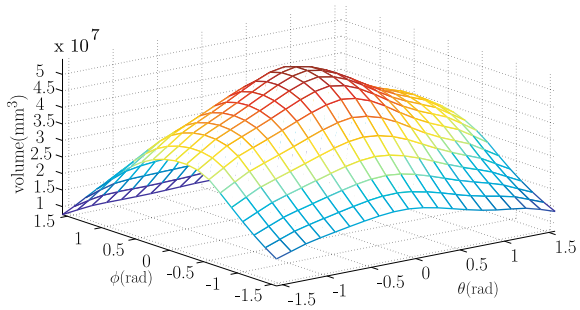

Fig. 20 Volume of the constant-orientation workspace with respect of (ϕ, θ) for the design presented in Table 1

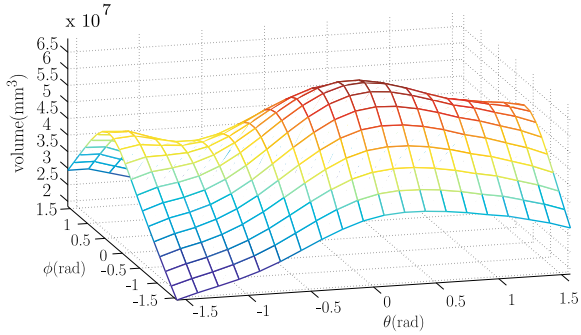

Fig. 21 Volume of the constant-orientation workspace with respect of (ϕ, θ) for the design presented in Table 2, $\{\mathcal{A}_1\mathcal{A}_1\}$

Upon performing the integration, it follows that:

$$\mathcal{D}_i = \begin{cases} -y'_l(z'_u - z'_l) & \text{for the left side boundary,} \\ y'_r(z'_u - z'_l) & \text{for the right side boundary,} \end{cases} \tag{43}$$

where (z'_l, z'_u) and (y'_r, y'_l) stand respectively for the z' (lower and upper) and y' (right and left) components of the line constituting the boundary of the constant-orientation workspace found by the algorithm. The above formulation for computing the volume of the workspace is integrated inside the algorithm for obtaining the boundary of the constant orientation workspace. Figures 20 and 21 represent respectively the volume of the constant-orientation workspace with respect of two permitted orientations, (ϕ, θ), for the designs presented in Tables 1 and 2.

5 Conclusion

This paper investigated the FKP and constant-orientation workspace of 5-DOF parallel mechanisms

(3T2R) with a limb kinematic arrangement of type RPUR. Two sets of simplified designs, (9) and (10), were presented whose FKP can be expressed either by a univariate expression or by a closed-form solution. Bohemian domes appeared in the geometrical interpretation of each limb and led to a CAD representation of the constant-orientation workspace. A geometric constructive approach was proposed, inspired from the one presented in [8], in order to find the boundary of the constant-orientation workspace The algorithm made it possible to find the volume of the constant-orientation workspace by applying the *Gauss Divergence Theorem* and provided some insight into the optimum synthesis of 5-RPUR parallel mechanisms. The principles of this paper can be applied equally well to the other types of symmetrical 5-DOF parallel mechanisms developed through the type synthesis, such as 5-PRUR, in order to obtain similar results for the FKP. Ongoing works includes the solution of the FKP in a univariate form for a general design and the optimum synthesis of the 5-RPUR.

Acknowledgements The authors would like to acknowledge the financial support of the Natural Sciences and Engineering Research Council of Canada (NSERC) as well as the Canada Research Chair program. The authors would also like to thank Ian Tremblay for his help in the preparation of the CAD model of the $\{\mathcal{A}_1\mathcal{A}_1\}$ design, Fig. 4.

References

1. Parallelmic, http://www.parallemic.org/
2. Bonev IA (2002) Geometric analysis of parallel mechanisms. PhD thesis, Laval University, Quebec, QC, Canada
3. Bonev IA, Gosselin CM (2000) Geometric algorithms for the computation of the constant-orientation workspace and singularity surface of a special 6-RUS parallel manipulator. In: Proceedings of the 2000 ASME design engineering technical conferences, DETC2002/MECH-34257, Montreal, QC, Canada (2002)
4. Bonev IA, Ryu J (2001) A geometrical method for computing the constant-orientation workspace of 6-PRRS parallel manipulators. Mech Mach Theory 36(1):1–13
5. Cheng L, Wang H, Zhao Y (2008) Analysis and experimental investigation of parallel machine tool with redundant actuation. In: Proceedings of the first international conference on intelligent robotics and applications: part I. Springer, Berlin, pp 179–188
6. Fang Y, Tsai LW (2002) Structure synthesis of a class of 4-DoF and 5-DoF parallel manipulators with identical limb structures. Int J Robot Res 21(9):799–810
7. Gao F, Peng B, Zhao H, Li W (2006) A novel 5-DOF fully parallel kinematic machine tool. Int. J. Adv Manuf Technol 31(1):201–207
8. Gosselin C (1990) Determination of the workspace of 6-DOF parallel manipulators. ASME J Mech Des 112(3):331–336
9. Gosselin C, Merlet JP (1994) The direct kinematics of planar parallel manipulators: special architectures and number of solutions. Mech Mach Theory 29(8):1083–1097
10. Huang Z, Li QC (2001) A decoupled 5-DoF symmetrical parallel mechanism, Patent pending, China, No 01122274.3
11. Huang Z, Li QC (2002) General methodology for type synthesis of symmetrical lower-mobility parallel manipulators and several novel manipulators. Int J Robot Res 21(2):131–145
12. Huang Z, Li QC (2003) Type synthesis of symmetrical lower-mobility parallel mechanisms using the constraint–synthesis method. Int J Robot Res 22(1):59–79
13. Hunt KH (1979) Kinematic geometry of mechanisms. Oxford engineering science series, vol 7
14. Husty ML (1996) An algorithm for solving the direct kinematics of general Stewart-Gough platforms. Mech Mach Theory 31(4):365–379
15. Husty ML, Zsombor-Murray P (1994) A special type of singular Stewart-Gough platform. In: Advances in robot kinematics and computational geometry, pp 449–458
16. Innocenti C (2001) Forward kinematics in polynomial form of the general Stewart platform. ASME J Mech Des, 123(2):254–260
17. Jin Q, Yang TL, Liu AX, Shen HP, Yao FH (2001) Structure synthesis of a class of 5-DOF parallel robot mechanisms based on single opened–chain units. In: Proceedings of the 2001 ASME conferences. DETC2001/DAC-21153. Pittsburgh, PA (2001)
18. Kong X, Gosselin C (2005) Type synthesis of 5-DOF parallel manipulators based on screw theory. J Robot Syst 22(10):535–547
19. Kong X, Gosselin C (2007) Type synthesis of parallel mechanisms, vol 33. Springer, Heidelberg
20. Lipkin H, Duffy J (1985) A vector analysis of robot manipulators. In: Recent advances in robotics. Wiley, New York, pp 175–241
21. Mbarek T, Barmann I, Corves B (2004) Fully parallel structures with five degree of freedom: systematic classification and determination of workspace. In: Proceedings mechatronics & robotics, pp 990–995
22. Merlet JP (1993) Algebraic-geometry tools for the study of kinematics of parallel manipulators. In: Angeles c J, Hommel G, Kovacs P (eds) Computational kinematics. Kluwer Academic, Dordrecht, pp 183–194
23. Merlet JP (1999) Parallel robots- open problems. In: 9th Int Symp of Robotics Research, pp 27–32
24. Merlet JP (2006) Parallel robots. Springer, Berlin
25. Piccin O, Bayle B, Maurin B, de Mathelin M (2009) Kinematic modeling of a 5-DOF parallel mechanism for semi-spherical workspace. Mech Mach Theory 44(8):1485–1496
26. Tale Masouleh M, Gosselin C (2009) Singularity analysis of 5-RPRRR parallel mechanisms via Grassmann line geometry. In: Proceedings of the 2009 ASME design engineering technical conferences. DETC2009-86261
27. Tale Masouleh M, Gosselin C (2008) Kinematic analysis and singularity representation of 5-RPRRR parallel mech-

anisms. In: Fundamental issues and future research directions for parallel mechanisms and manipulators Montpellier, France, (2008), pp 79–90.
28. Tale Masouleh M, Husty M, Gosselin C (2010) A general methodology for the forward kinematic problem of symmetrical parallel mechanisms and application to 5-PRUR parallel mechanisms (3T2R). In: Proceedings of the 2010 ASME design engineering technical conferences, DETC2010-28222
29. Tale Masouleh M, Husty M, Gosselin C (2010) Forward kinematic problem of 5-PRUR parallel mechanisms using study parameters. In: Advances in robot kinematics: motion in man and machine. Springer, Berlin, pp 211–221
30. Tale Masouleh M, Saadatzi MH, Gosselin C, Taghirad HD (2010) A Geometric constructive approach for the workspace analysis of symmetrical 5-PRUR parallel mechanisms (3T2R). In: Proceedings of the 2010 ASME design engineering technical conferences. DETC2010-28509
31. Wang J, Gosselin C (1997) Kinematic analysis and singularity representation of spatial five-degree-of-freedom parallel mechanisms. J Robot Syst 14(12):851–869
32. Zhu SJ, Huang Z (2007) Eighteen fully symmetrical 5-DoF 3R2T parallel manipulators with better actuating modes. Int J Adv Manuf Technol 34(3):406–412